Hydration of hydroxyl and amino groups examined by molecular dynamics and neutron scattering

Jana Hladílková,[1] Henry E. Fischer,[2] Pavel Jungwirth[1] and Philip E. Mason[1]*

Institute of Organic Chemistry and Biochemistry, Academy of Sciences of the Czech Republic, Flemingovo nám. 2, 16610 Prague 6, Czech Republic

Institut Laue-Langevin, 71 avenue des Martyrs, CS 20156, 38042 Grenoble cedex 9, France

[*]Corresponding author: e-mail philip.mason@uochb.cas.cz
KEYWORDS, amine, alcohol, neutron scattering, molecular dynamics, solution.

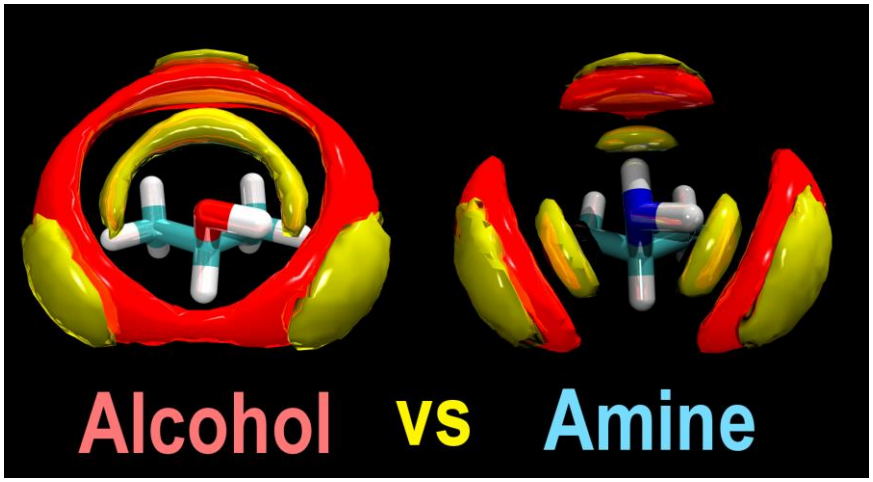

Abstract

Neutron diffraction with isotopic substitution was performed on aqueous solutions of isopropanol and isopropylamine. The difference between these two measurements primarily contains information about the different hydration of the alcohol and amino group. This data is used as a test of the accuracy of molecular dynamic simulations of the same systems. Having established the level of accuracy of the modeling, it is employed as an interpretive tool for the experimental data. Even though the alcohol and the amine possess comparable hydrogen bonding capabilities, consisting respectively of either two hydrogen bond acceptors and one donor, or two hydrogen bond donors and one acceptor, we find significant differences in the hydration of the hydroxyl and amino groups.

Introduction

Despite the fact that alcohols and amines are ubiquitous in nature, there is relatively little structural data available that compares directly aqueous solvation of the hydroxyl and amino groups. Alcohols and amines are electronically practically isomorphic and both can in principal form three unfrustrated hydrogen bonds (H-bonds). Alcohol can be a donor of one H-bond and an acceptor of two, while amine can be a donor of two H-bonds and an acceptor of only one. By definition, in pure water every hydrogen bond donor must also have a hydrogen bond acceptor. However, even here the fact that the water molecule has C_{2V} and not tetrahedral symmetry means that the three dimensional structures of donors and acceptors differ from each other.[1]

As both alcohols and amines possess important functional groups in many biological systems, a better understanding of amine-water and alcohol-water hydrogen bonding will be of a broad importance. Hydroxyl groups are far more common than amines, occurring in sugars,[2] amino acids,[3] and in many smaller biological molecules such as choline.[4] One reason why amines are not found in biological systems in large quantities is due to the fact that they tend to protonate, making aqueous solutions basic.[5] There is, however, a crucial importance of amino groups in specific niche roles such as in neurotransmitters[6]. While there have been several computational studies of amines,[3, 7, 8] relatively few of them have contained comparison to structural experimental data such as from neutron scattering measurements.[9] It is also true that amines have been notoriously difficult to parameterize in the past, as the resulting force fields often failed in reproducing all the requested properties of amines in aqueous solution.[8]

We examine here a simple liquid alcohol (isopropanol, *ipal*) and the structurally corresponding amine (isopropyl amine, *ipam*) in order to directly compare their hydration properties. These two molecules were chosen being both highly symmetric and having very similar structures (with the exception of the functional group). On top of that, both are liquids

at room temperature with high solubilities in water. We first perform neutron diffraction with isotopic substitution (NDIS)[10, 11] on aqueous solutions of both isopropanol and isopropyl amine. By direct comparison of the measured spectra of the two species, we are able to determine the pertinent differences in their hydration. Molecular dynamics is first used as a heuristic test for the veracity of the force field used in the simulations and, secondly, as an interpretive tool for understanding the neutron scattering data.

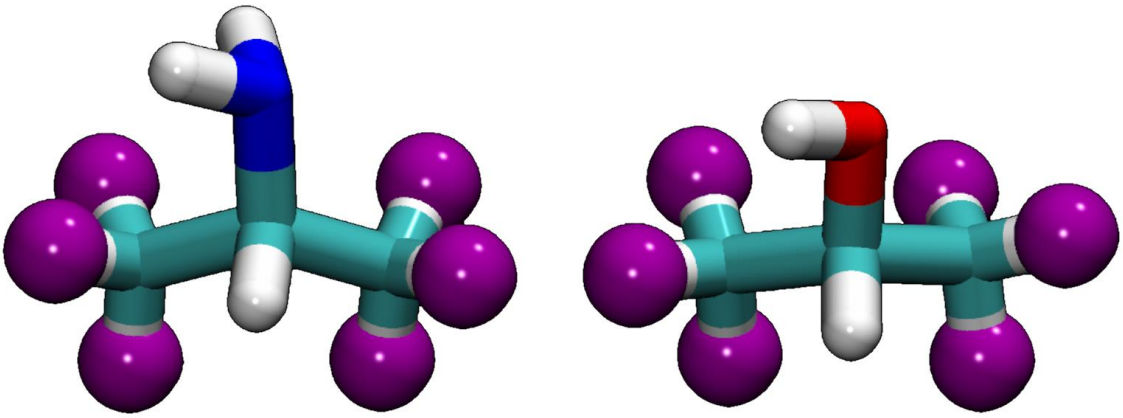

Figure 1. The molecular structure of isopropyl-amine (*ipam*) is shown on the left and that of isopropanol (*ipal*) on the right. In each case the hydrogen nuclei substituted in the NDIS experiments (H_{sub}) are highlighted in purple.

Experimental Methods

The first-order NDIS experimental results presented here were obtained by substituting the six non-exchangeable methyl hydrogens on both *ipal* and *ipam (*Figure 1). These hydrogens are hereafter termed H_{sub} (for substituted hydrogen). The non-exchangeable hydrogen attached to C2 and the exchangeable hydrogens (including both the exchangeable hydrogens

on the water and the -OH or -NH_2 groups) are denoted as H_{non} and H_{ex} respectively. Oxygens on water and *ipal* are termed O_w and O_{ipal}, respectively. Nitrogen on *ipam* is referred to as N and carbon atoms are labeled as C.

In order to conduct a NDIS experiment, two 'chemically' identical solutions that vary in the isotopic concentration of at least one element are required. We substituted the non exchangeable methyl hydrogens of the isopropyl groups of *ipal* and *ipam*, mixed with water (D_2O) in the ratio of 3:55.55 (referred to as 3m for simplicity). 3000 mg of D_2O (99.9 % atom percent D, supplied by ILL) was placed in a fresh 5 ml naglene tube, where 487 mg of natural *ipal* was added to it. This tube was then sealed and shaken, and allowed to stand for 30 minutes to thermally equilibrate before being placed in a Ti/Zr null-alloy neutron scattering container. The second solution was prepared in an identical manner, but using 3000 mg of the same D_2O and 534 mg of d6 *ipal*. The sample preparation procedure of the *ipam* solutions was identical, but half the volume of each solution was made (1500 mg of D_2O was used in each case). For both *ipal* and *ipam* the exchangeable hydrogens were ^1H. This does mean that the average coherrent neutron scattering length for Hex between these two samples is very slightly different. An identical 3m *ipam* solution was prepared in H_2O and its pH was measured as 12.9. This equates to about 1 *ipam* in 30 being protonated.

Thanks to the high neutron counting and excellent stability of the D4C neutron diffractometer[12], it was necessary to acquire data on these high contrast samples for only ~2 hours each. These raw total neutron scattering patterns (measured at a wavelength of 0.7 Å) were corrected for multiple scattering and absorption effects prior to being normalized versus a previously characterized sample (a ~6mm vanadium cylinder). This produced the total scattering patterns (S(Q)) for each solution (d6 *ipal* and h6 *ipal* in D_2O, and d6 *ipam* and h6 *ipam* in D_2O). The first-order difference was then taken between these practically isomorphic

solution to yield the first-order NDIS measurement for the *ipal* and *ipam* solutions ($\Delta S_{ipal}(Q)$ and $\Delta S_{ipam}(Q)$). These can be expressed as follows:

$$\Delta S_{ipal}(Q) = 66.7\, S_{HsubHex}(Q) + 29.4\, S_{HsubOw}(Q) + 1.59\, S_{HsubOipa}(Q) + 5.46\, S_{HsubC}(Q) - 1.02\, S_{HsubHnon}(Q) + 2.41\, S_{HsubHsub}(Q) - 104.5 \quad (1)$$

$$\Delta S_{ipam}(Q) = 63.7\, S_{HsubHex}(Q) + 28.5\, S_{HsubOw}(Q) + 2.49\, S_{HsubN}(Q) + 5.30\, S_{HsubC}(Q) - 0.99\, S_{HsubHnon}(Q) + 2.34\, S_{HsubHsub}(Q) - 101.5 \quad (2)$$

In each case the neutron scattering prefactors (in units of millibarns) for the g(r)s are calculated using the formula $2c_{\mathrm{Hsub}}c_{\alpha}\Delta b_{\mathrm{Hsub}}b_{\alpha}$ where c is the atomic concentration of that nuclei, b is the average coherent neutron scattering length of that nuclei, and Δb_{Hsub} is the difference in the coherent neutron scattering lengths of ^{2}H and ^{1}H (deuterium and protium). The self-term is different ($c_{\mathrm{Hsub}}{}^{2}(b_{\mathrm{D}}{}^{2} - b_{\mathrm{H}}{}^{2})$) for reasons that are described elsewhere.[13]
These functions can be Fourier transformed to yield the corresponding *r*-space functions (see equations 3 and 4). The formal mathematical relationship between the Q and r space data is described elsewhere.[14]

$$\Delta G_{ipal}(r) = 66.7\, g_{HsubHex}(r) + 29.4\, g_{HsubOw}(r) + 1.59\, g_{HsubOipa}(r) + 5.46\, g_{HsubC}(r) - 1.02\, g_{HsubHnon}(r) + 2.41\, S_{HsubHsub}(Q) - 104.5 \quad (3)$$

$$\Delta G_{ipam}(r) = 63.7\, g_{HsubHex}(r) + 28.5\, g_{HsubOw}(r) + 2.49\, g_{HsubN}(r) + 5.30\, g_{HsubC}(r) - 0.99\, g_{HsubHnon}(r) + 2.34\, g_{HsubHsub}(r) - 101.5 \quad (4)$$

Simulation Methods

Classical molecular dynamics simulations of isopropyl alcohol and isopropyl amine in water bulk solutions were performed with Amber11[15] simulation package. In order to reproduce correct densities of our solutions, NVT ensemble was applied with size of the box complying with experimentally established values (0.10034 atoms $Å^{-3}$ and 0.1013 atoms $Å^{-3}$ for *ipal* and *ipam*, respectively). 36 ipal or 56 ipam molecules were solvated in 667 or 1036 water molecules, yielding large enough systems to exclude artifacts due to finite sizes of the unit cells. The OPLS force field[16] was used for investigated molecules and the SPC/E model for water.[17] In order to obtain converged radial and spatial distribution functions, 30 ns production runs with 1 fs time step were conducted at ambient temperature (Berendsen thermostat)[18] after 1 ns of equilibration. 3D periodic boundary conditions were applied with a 10 Å cutoff for long-range interactions using the particle mesh Ewald (PME) method.[19]

Results

From the neutron scattering data the first-order difference NDIS functions for both *ipam* and *ipal* were calculated in Q-space. From Figure 2 it is clear that there are many similarities between the first-order differences of *ipam* and *ipal*. This is principally because these molecules have very similar topologies, which is, of course, one of the reasons why these molecules were chosen. The most important aspect of this study is to examine in detail the small differences between these two sets of data, as they contain the most interesting information about the different hydration of the hydroxyl and amino groups.

In order to interpret these experimental measurements, the functions $\Delta G_{ipal}(r)$ and $\Delta G_{ipam}(r)$ were calculated from the molecular dynamics (Figure 3). The first three peaks (in black) are essentially identical, because they relate to the structure of the isopropyl groups which are the same for both *ipal* and *ipam* at almost identical concentrations of H_{sub}. For example, peaks at 1.1, 1.8, and 2.3 Å are due to **H_{sub}-C**, **H_{sub}**-C-**H_{sub}**, and **H_{sub}**-C-**C** correlations, where in bold

we represent the atoms in the pairwise correlation. If these peaks were integrated and converted into coordination numbers, they would yield identical values. The first conspicuous difference between $\Delta G_{ipal}(r)$ and $\Delta G_{ipam}(r)$ functions is the peak at ~2.8Å, which is primarily due to the molecular correlation $H_{sub}O_{ipa}$ in *ipal*, and $H_{sub}N$ in *ipam*. While the intramolecular correlations have exactly the same coordination number in each solution, the apparent size of the correlation varies as the coherent scattering length of nitrogen is almost twice that of oxygen (9.4 versus 5.8 fm). The second clear difference occurs in the region of 3.5 - 4.5Å, where $H_{sub}H_{ex}$ correlation peaks. As the Hex atoms are directly involved in hydrogen bond formation, we will discuss those results later in more detail. In contrast, the $H_{sub}O$ components seem almost identical for both *ipam* and *ipal*.

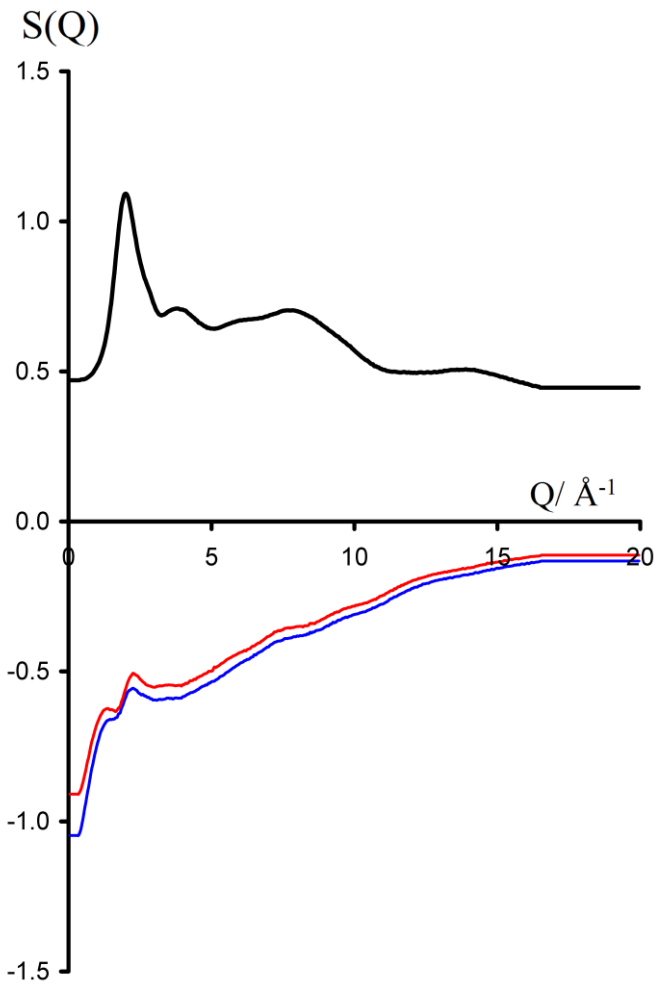

Figure 2. The total experimental scattering pattern for *ipal* (d6) in D_2O is shown in black for reference. The first-order differences for *ipam* and *ipal* are shown in red and blue, respectively. The slight overall gradients on these first-order differences are due to the Placzek effect.[20] In each case the first-order difference is of comparable proportions to the total scattering. It is immediately clear from this scattering data that the molecular and solution structures of *ipal* and *ipam* are very similar to each other. The lower and upper Q range of the experimental data is 0.5 and 16.5 $Å^{-1}$ respectively. There is no recorded data beyond these values.

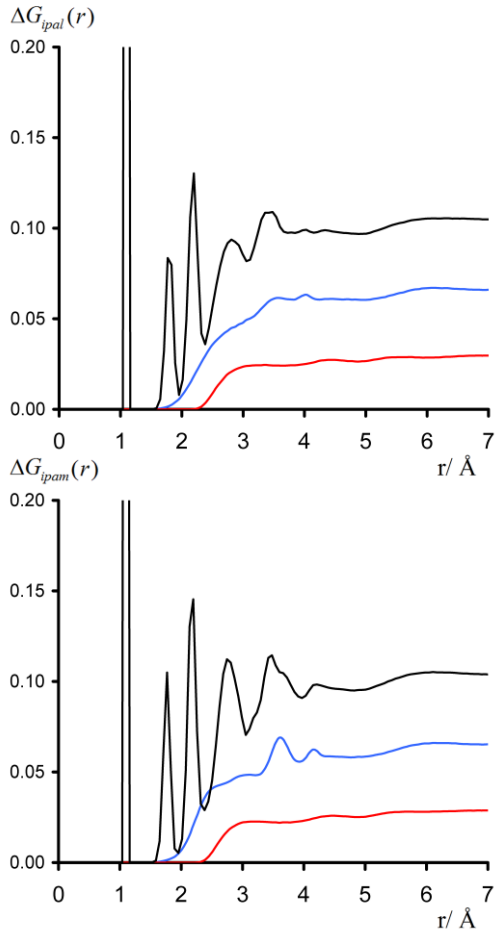

Figure 3. The functions $\Delta G_{ipal}(r)$ and $\Delta G_{ipam}(r)$ as calculated from the MD simulations. All the peaks up to ~2.2 Å are very similar to each other as the molecular geometries of both *ipal* and *ipam* are to a large extent comparable. Components of the functions $\Delta G_{ipal}(r)$ and $\Delta G_{ipam}(r)$ due to $H_{sub}H_{ex}$ and $H_{sub}O_w$ are shown in blue and red, respectively. The correlations of the substituted nuclei to O_w are more similar to each other for *ipal* and *ipam* than those for the H_{ex} atoms.

Discussion

Analysis of the second order difference function by component

A useful analysis for the subject under study involves the direct subtraction of $\Delta G_{ipam}(r)$ from $\Delta G_{ipal}(r)$. When this is performed (with a slight modification to correct for number densities, see equations 5 and 6), the molecular structure of the isopropyl group, assuming its identical conformational populations for both molecules, vanishes from the difference. Consequently, the small remaining residual contains the most important information about the differences in hydration shell of the investigated functional groups. This technique is very similar to the internal coordination number concentration invariance (ICNCI) approach[21]. If both of the first-order differences ($\Delta G(r)$) are multiplied by a factor composed of the atomic concentration of the substituted nuclei, and the number density of the solution (see equation 5), then a direct subtraction of these products will leave a residual double-difference function. This function will contain no correlations due to the intramolecular structure of the molecular on which the substitution is conducted and is primarily a structural measure of the difference in solvation between the alcohol and amino group.

Specifically, $\Delta\Delta G_{ipaX}(r) = \frac{\Delta G_{ipal}(r)}{c_{Hsub(ipal)} \bullet n_{ipal}} - \frac{\Delta G_{ipam}(r)}{c_{Hsub(ipam)} \bullet n_{ipam}}$ (5)

When the comparison is done in Q space this multiplicative prefactor is slightly different (equation 6).[11]

$$\Delta\Delta S_{ipaX}(Q) = \frac{\Delta S_{ipal}(Q)}{c_{Hsub(ipal)}} - \frac{\Delta S_{ipam}(Q)}{c_{Hsub(ipam)}} \quad (6)$$

One significant advantage to the ICNCI method is that it by default almost completely cancels out the Placzek effect. The Placzek effect usually gives the Q-space data the appearance of 'climbing a hill' (see Figure 2). The intensity of the Placzek effect is primarily determined by the concentration of ^{1}H in the sample. This is a broad, and difficult to define function with an approximate wavelength of about 80Å^{-1}, and when Fourier transformed by itself produces very large unphysical r-space features almost exclusively below 0.5 Å. This can be problematic as these large features can produce 'ringing' artifacts that can make interpretation of the r-space data difficult. By inspection of equation 6, it is clear that the ICNCI function is almost exactly a 1:1 difference of the two Q-space functions, and because of the similar Placzek effect in the two experimental data sets (see Figure 2), it is clear that the ICNCI method will intrinsically mostly eliminate the Placzek effect from the data. In this case this cancellation occurs because the Placzek effect is primarily determined by the atomic concentration of ^{1}H in the ^{1}H substituted sample. This concentration is almost exactly the same for the *ipam* and *ipal* first order differences, so a difference between these two will almost exactly cancel out this troublesome effect. Indeed this cancellation can work as a form of internal consistency check for the experimental data, as a large residual Placzek effect in the ICNCI function would suggest that there is an error in the experiment.

First, we apply the ICNCI technique to the simulation data to verify the isomorphic approximation of the two isopropyl groups. Second, we aim to identify the origins of the small hydration differences of the hydroxyl and amino functional groups. Every correlation in $\Delta G_{ipal}(r)$ has a corresponding element in $\Delta G_{ipam}(r)$, e.g., g_{HsubOw}(r) in *ipal* corresponds to g_{HsubOw} (r) in *ipam*, $g_{HsubOipa}$(r) in *ipal* corresponds to g_{HsubN}(r) in *ipam*, etc. Therefore, the

contributions of these individual elements (in red) to the total double-difference function (in black) can be dissected one by one (Figure 4). This analysis can be done both in real and reciprocal spaces.

While examining all the rest of the simulation data, as well as the experimental data, it is necessary to bear in mind the relationship between Q and *r*-space.[21] Intramolecular correlations tend to be narrow peaks at lower *r*, manifesting themselves as weakly damped sine waves in Q-space, where the frequency of that sine wave defines the peak position in r space. Intermolecular correlations tend to be broad features at higher *r* in *r*-space, and manifest themselves as more severely damped higher frequency features in Q-space. As a general rule, all of the data on intermolecular correlations occurs below 5 $Å^{-1}$.

Correlations to H_{non}, C, N, and O_{ipa}

The examination of the H_{sub}-C component of the double-difference function shows that there are actually minor changes in the structure of the isopropyl group between *ipal* and *ipam*. Very small differences in the peak positions of the H_{sub}-C correlations appear as a large negative spike followed by an equally sized large positive spike at a very similar *r* value (Figure 4). Obviously, if the molecular structures were entirely isomorphic, these differences would cancel completely. It is clear that the H_{sub}-C component is only a small contributor to the Q-space double-difference function (Figure 4). For the H_{sub}-C component, the majority of the signal found in the double-difference function is in the low-Q region which corresponds to different long range structuring of the *ipal* and *ipam* solutions.

The H_{sub}-O_{ipa}/ H_{sub}-N difference is a major component of the double-difference function, although this does not correspond to significant structural differences between *ipam* and *ipal (vide infra).* It will for convenience be assumed that these molecules adopt the optimal entirely staggered conformations (Figure 1). There are two intramolecular peaks for either of

the $H_{sub}O_{ipa}$ or $H_{sub}N$ correlations because of the broken symmetry of the *ipal*/ *ipam* motifs. These two functions are almost identical consisting of two peaks at 2.6 and 3.3 Å corresponding to the two principal intramolecular correlations of either $H_{sub}O_{ipa}$ or $H_{sub}N$. The peak at 2.6 represents four out of the six H_{sub} hydrogens while the peak at 3.3 Å represents the remaining two H_{sub} hydrogens. It should be noted that the $H_{sub}O_{ipa}$ peaks are slightly broader than the $H_{sub}N$ peaks. However, by far the largest reason why this difference between the $H_{sub}O_{ipa}$ and $H_{sub}N$ components plays such a significant role in the double-difference function is that the $g_{HsubN}(r)$ has a larger neutron scattering prefactor than the $g_{HsubOipa}(r)$ (equations 1-4). As we already mentioned, the neutron scattering length of nitrogen is almost twice that of oxygen, therefore, the $g_{HsubOipa}(r)$ / $g_{HsubN}(r)$ component of the double-difference function principally resembles a negative version of the function $g_{HsubN}(r)$. The difference between $H_{sub}O_{ipa}$ and $H_{sub}N$ is the largest component to the double-difference function in the higher Q region of the Q-space data.

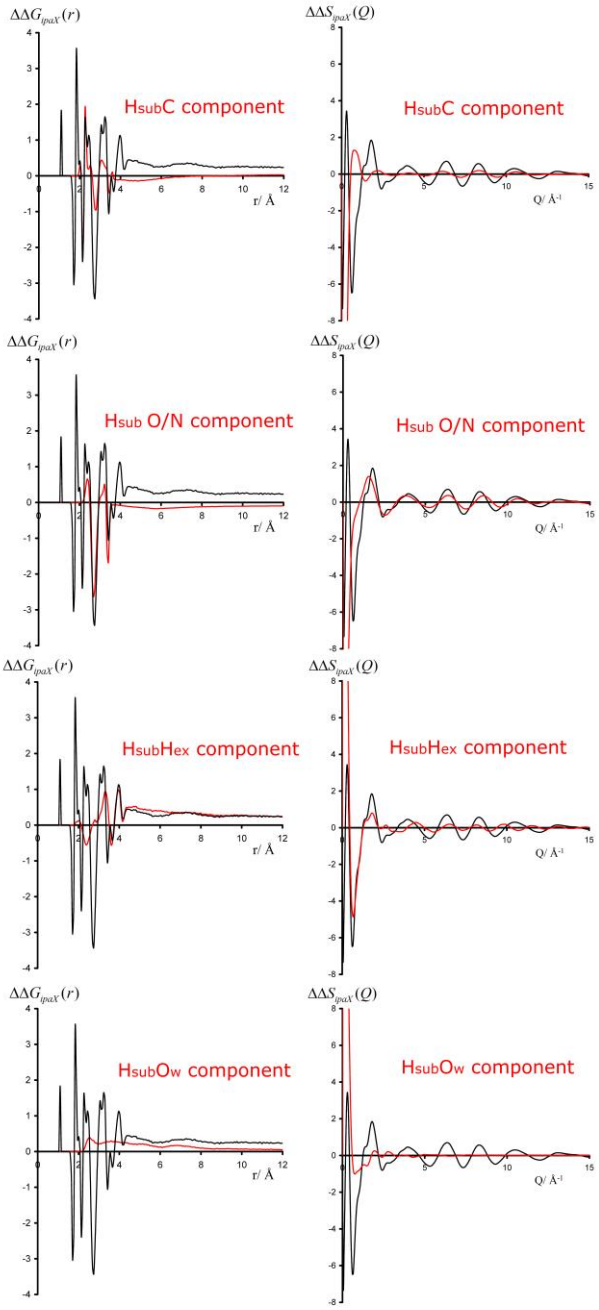

Figure 4. The real space function $\Delta\Delta G_{ipaX}(r)$ (black) is shown on the left and the reciprocal space function $\Delta\Delta S_{ipaX}(Q)$ (black) is shown on the right- both calculated from the molecular dynamics simulations. The element of the total double-difference due to the component labeled on the figure in red is shown as a red line. The reciprocal space versions of these functions is shown on the right.

Correlations to H_{ex} and O_w

It follows from the above results that the $H_{sub}C$ and $H_{sub}N/O$ components of the double-difference function are only of peripheral interest to this study, as we primarily focus on the differences in hydration of the alcohol and the amine. The contribution of the $H_{sub}H_{ex}$/ $H_{sub}O_w$ components of the double-difference function are probably the most interesting elements of this study as they contain most of the information about the difference in hydration of the hydroxyl and amino group. This term also contains information about the different dispositions of the exchangeable hydrogens on the electronegative atom of *ipal* or *ipam*. In each case a hydrogen attached to the electronegative atom can occupy one of three energetically favorable positions. Two of them are structurally degenerate (*gauche* relative to the H_{non} on C2) and one is unique (*trans* relative to H_{non}). The *gauche* position provides six correlations to the H_{sub} atoms, while the *trans* position produces only three correlations for the H_{sub} atoms. Some of these correlations are so close to each other that they would not produce peaks that could be resolved above the thermal population of the rotational states of the molecules. In order to visualize the contributions of the individual H_{ex} atoms to the function $g_{H_{sub}H_{ex}}(r)$, the contributions of the nearest 20 H_{ex} atoms to O_{ipal} or N respectively in the function $g_{H_{sub}H_{ex}}(r)$ were calculated (Figure 5).

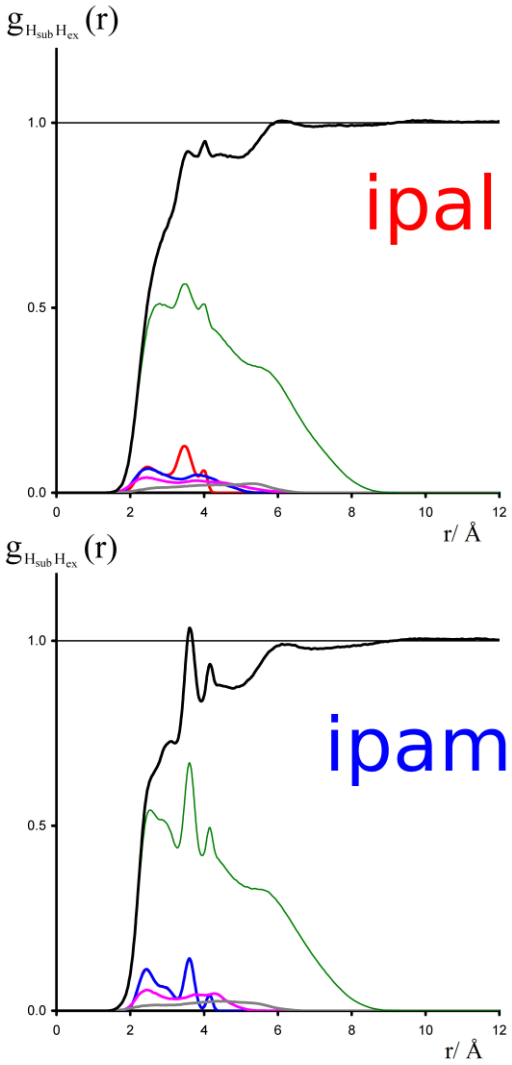

Figure 5. The functions $g_{HsubHex}(r)$ are shown in black, as calculated from the MD simulations for *ipal* (upper) and *ipam* (lower). Contribution to this function from the nearest 20 H_{ex} atoms to either N or O_{ipa} is shown in green and the nearest H_{ex} atom to either N or O_{ipa} is shown in red. For both the *ipal* and the *ipam* this hydrogen is part of the alcohol and amine respectively. The second nearest atom to either N or O_{ipa} is shown in blue, the third in purple, and the forth in grey. The reason there is apparently no red line visible for *ipam* is that it is exactly the same as the blue line.

The nearest correlation from a Hex atom to the heteroatom of the *ipal* is due to the hydroxyl proton, while the nearest two correlations for the *ipam* function are due to the amine protons. The second and third nearest correlations for the *ipal* group are due to hydrogen bond donors to the electronegative atom, while this is only true for the third nearest correlation for the *ipam* group. The combination of the lack of symmetry of the isopropyl group, along with the two possible positions which the amine/alcohol exchangeable hydrogens can occupy, makes interpretation of the function $g_{HsubHex}(r)$ extremely difficult. This interpretation would have been easier if a more symmetric group had been used like methanol/methylamine. This option was not pursued at the time as methyl amine is a gas and would have made the sample preparations more complicated. Nevertheless, information about the conformation of the hydroxyl and amine groups can be directly extracted from the molecular dynamics simulations. This is easily observed from the density maps calculated for these systems (Figure 6). It is found that the amine hydrogens tend to occupy all three rotationally distinct positions equally, while there is a significant preference for the hydroxyl hydrogens to occupy the two degenerate *gauche* positions. Interestingly, the position of the first three oxygens surrounding these groups is also significantly different, with these oxygens occupying more distinct positions with the amine when compared to the alcohol.

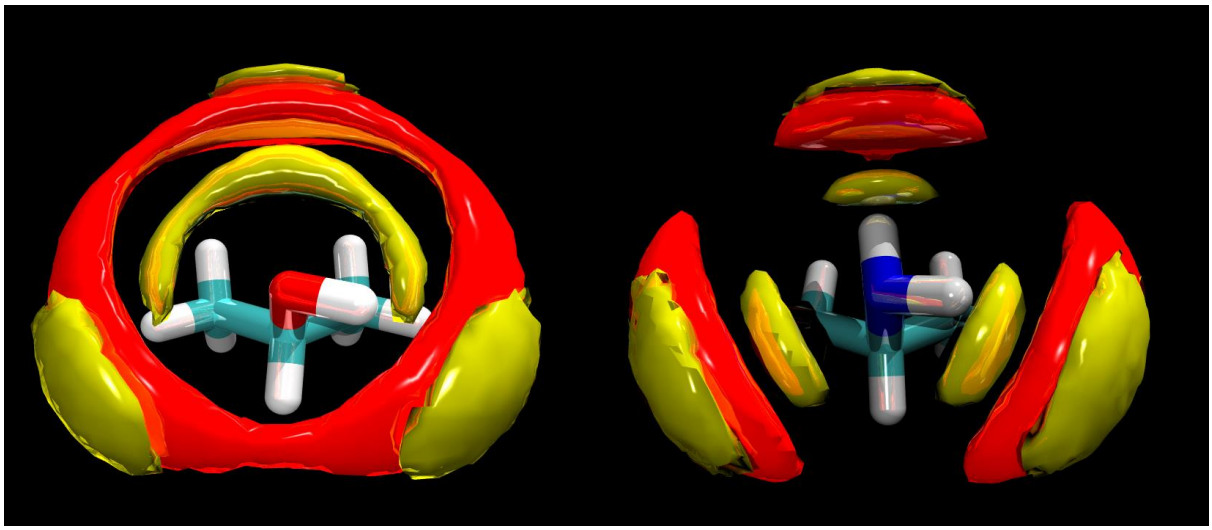

Figure 6. The density maps of water oxygen (red) and water hydrogen (yellow) are shown around either *ipal* (left) or *ipam* (right). The level of the contour is 0.075 atoms $Å^{-3}$ and 0.15 atoms $Å^{-3}$ for oxygen and hydrogen respectively. Clearly from the closest yellow cloud (hydrogen bond on water being a donor to the alcohol or amine) the alcohol mostly occupies the two degenerate positions *gauche* to H_{non}, while in the amine, all three positions are approximately equally occupied.

Before examining the comparison between the ICNCI functions from both the experiment and MD, it may be sensible to answer the obvious question, 'why not just compare the first order difference functions (eg $\Delta G_{ipam}(r)$) from the molecular dynamics to that from the experimental data?' The problems with this comparison very nicely highlight many of the reasons why we developed the technique of ICNCI. Historically direct comparison between MD and NDIS measurements of aqueous solutions, where the NDIS substitution was performed on a molecular structure have been problematic. This primarily stems from the fact that molecular correlations give very large, very sharp features in r-space. This can be seen in the function $\Delta G_{ipam}(r)$ generated from the MD data (upper left panel Figure 7), which may, however, overestimate this sharpness due to lack of nuclear quantum effects which could broaden the intramolecular peaks. The experimental measurement on instruments such as D4C do not have the Q-range to fully define the sharpness of these features. This point can be demonstrated by back-Fourier transforming the MD function for $\Delta G_{ipam}(r)$ to

$\Delta S_{ipam}(Q)$. Sharp features in r-space tend to produce features that extend out to high Q. The fact that the Q space data generated from the back transform of the function $\Delta G_{ipam}(r)$ extends out beyond the high Q limit of the experimental measurement (~16.5Å) suggests that the experimental measurement will be resolution limited (upper right panel, Figure 7). A fairer comparison of the MD and neutron scattering data is to Fourier transform both data sets using the experimental Q range (0.3-16.5 Å). The comparison of the original $\Delta G_{ipam}(r)$ generated from the MD, and the same data set after it has been Fourier transformed with the experimental Q-range, allows the full extent of complications of Fourier transform artifacts from sharp molecular correlations to be seen. This is most notable on the peak at 1.1 Å corresponding to the Hsub-C correlation. These artifacts can be somewhat removed by setting the new $\Delta G_{ipam}(r)$ data sets (middle left Figure 7) to the low r limit in the range 0-2 Å (thereby removing these frequency elements, and a large part of the artifacts that come with them from the data set) and then back Fourier transforming both data sets to get a Fourier filtered version of $\Delta S_{ipam}(Q)$ (middle right Figure 7). This can be justified as only intramolecular correlations, which are of little interest, are deleted and further means that what is left consists mostly of the more interesting intermolecular correlations. This deletion also has the effect of removing almost all the Placzek effect from the experimental data and greatly improves the comparison between the MD and experimental data sets. Lastly the data can be again Fourier transformed into real space to inspect for how this has affected the comparison. Again it is found that the 'deletion' of the peaks in the region 0-2 Å has not only removed these peaks, but most of the artifacts associated with them. The comparison between the MD and experimental data is satisfactory, but nonetheless the sharp intramolecular correlations have the effect of obscuring the underlying hydration structure that we are primarily interested in. What is really needed is a method that can simply remove these sharp peaks from the data, and this was the prime reason why the method of ICNCI was developed. What is left after the method of ICNCI has been applied, should in principal contain no intramolecular correlations, with all the residual signal being due to the differences between the hydration of the two generic targets used in the technique. All of this is achieved with no complicated data analysis, or Fourier transforms, smoothing or filtering, but only by the numerical subtraction of four data sets.

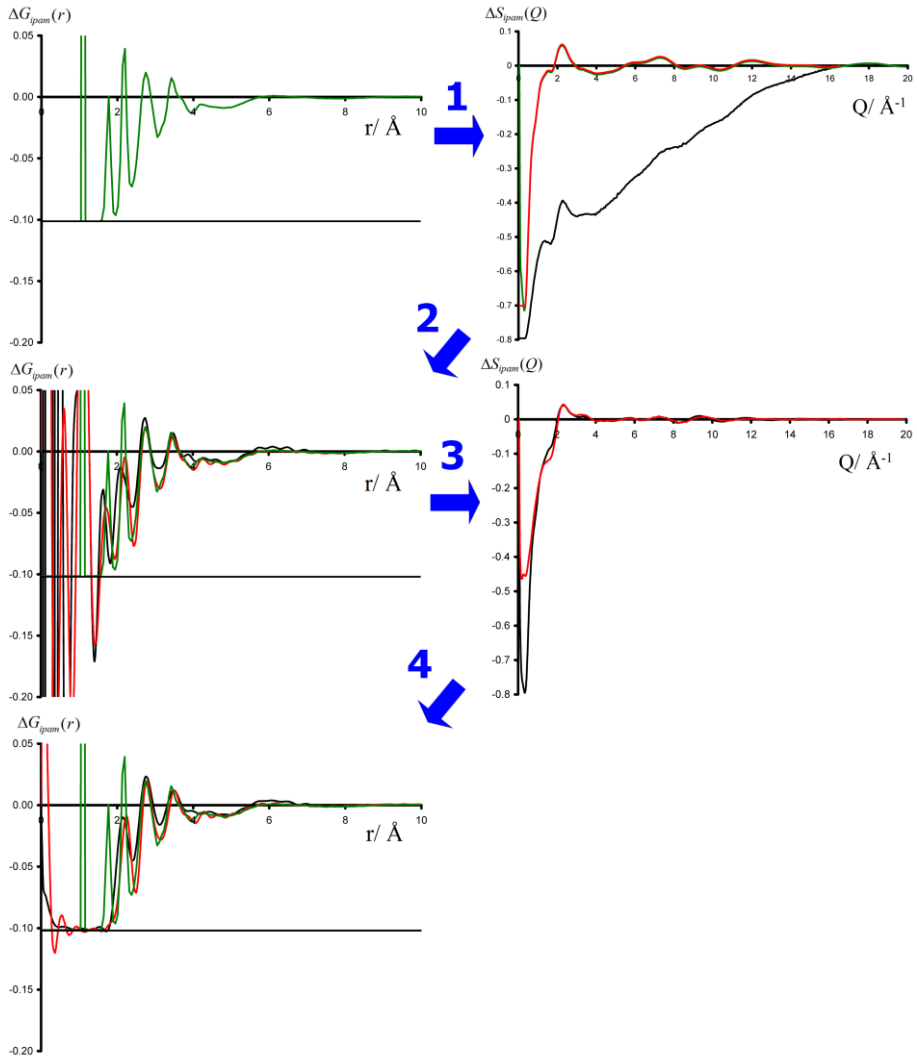

Figure 7. Upper left green is shown the function $\Delta G_{ipam}(r)$ generated from the MD data. This green data set is exactly the same for all the panels on the left. Blue arrow 1 represent the upper left data being back Fourier transformed to the function $\Delta S_{ipam}(Q)$ (upper right green). Also shown in the upper right panel is the raw function $\Delta S_{ipam}(Q)$ calculated from the experimental data (black) and the MD version of this function after it has had the experimental Q range applied to it (0.3-16.5 Å, red). Blue arrow 2, the black and red data sets (both with the experimental Q-range) are Fourier transformed to their corresponding real space functions in the middle left panel. Blue arrow 2, the black and red r-space data in the middle left panel is set to the low r limit (101mb, see eq 4) in the region 0-2 Å, and back fourier transformed to Q-space. Blue arrow 4, red and black data from the middle right panel is fourier transformed to r-space.

The MD reconstruction of the double-difference function by components (Figure 4) allows us to more accurately interpret the features in the experimental measurement (Figure 8). The higher Q region (5 - 15 $Å^{-1}$) contains little data of interest, as it is primarily due to nitrogen having a larger coherent scattering cross section than oxygen. The majority of the lower Q signal (below 5 $Å^{-1}$) is due to the different ordering of H_{ex} around the substituted nuclei. The high Q MD data corresponds very well in 'frequency' to the higher Q experimental data, but the experimental data attenuates more at higher Q than the MD data. This is a widely observed effect when H/D substitution is employed and compared to experimental data.[11] Its origins are in part in the quantum uncertainty in the position of the hydrogen atom, not accounted for within the classical MD simulations. The lower Q signal mostly reproduces differences in the H_{sub}-H_{ex} correlations between these two solutions. For the high and low Q data, the agreement between the MD and experiment is very acceptable; there appears to be no appreciable failings of the molecular dynamics in this case.

It may be argued that this comparison is somewhat problematic due to the fact that the experimental and simulations systems of *ipam* are not identical. This is because in the experimental system approximately 3 % of the *ipam* moieties are protonated while in the simulation system, none of them are. However, having a 3 % contamination of the *ipam* simulation, by a group that would have a very similar structure to the unprotonated ipam group, would not present a significant (beyond statistical change) error in the current study. It should be kept in mind that this double-difference function constitutes only a very small component of the total scattering, but it contains the most pertinent information on the difference of the hydration of the *ipam* and *ipal* functional groups.

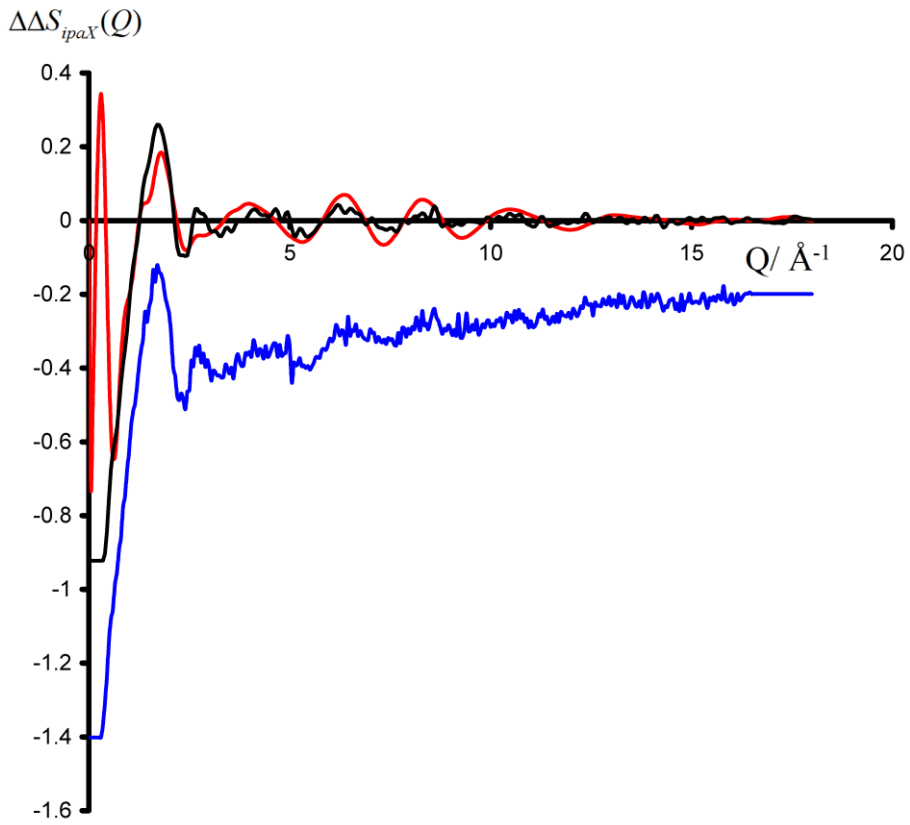

Figure 8. The function $\Delta\Delta S_{ipaX}(Q)$ as calculated from the simulation is shown in red with the same 'raw' function obtained from the experiment shown in blue. Shown in black is the 'raw' experimental function after a minor Fourier filtering to remove all unphysical real space features below 0.5 Å. For this latter function, artefactual data below the low Q limit of the diffractometer (~0.3Å^{-1}) has been set to a flat line.

Having verified that the simulations reliably reproduce the experimental data, we now use the simulations to examine quantitatively the hydrogen bonding aspects of hydration of *ipam* and *ipal*. For each electronegative atom the number of H-bonds was calculated (employing standard distance and angle cutoffs of 3.5 Å and 120º). It was found that on average the hydroxyl group of *ipal* forms 2.71 hydrogen bonds while the amine group of *ipam* forms 2.53.

	ipal as Hbond acceptor	*ipal* as Hbond donor		*ipam* as Hbond acceptor	*ipam* as hbond donor
Oipa	0.055	0.055	N	0.033	0.033
Ow	1.66	0.94	Ow	1.21	1.26
Total Hbonds	1.72	0.99		1.24	1.29

Table 1. The hydrogen bonding statistics from the *ipal* and *ipam* MD simulations. In each case total numbers have been broken down by donor and acceptor contributions.

In terms of number of hydrogen bonds the hydroxyl group of *ipal* is a better former of hydrogen bonds than the amino group of *ipam*. If it is assumed that all hydrogen bonds are of comparable strength, then this implies that the hydroxyl group is more strongly hydrogen bonded than the amino group. Naturally caution should be exercised when using such crude approximations like 'if all hydrogen bonds are assumed to be of comparable strength'. For instance even within this study it is found that the oxygens seem to be more ordered around the amino group than around the hydroxyl group (see Figure 6). Nonetheless the main conclusion of this simple approximation that 'if all hydrogen bonds are assumed to be of comparable strength' is in line with many observations about the physical properties of alcohols and amines. Assuming that the stronger the hydrogen bonding in a species, the higher its boiling point is, then the results are generally consistent with the physical properties of the two species, where pure *ipal* has a boiling point of ~83 ^{o}C while *ipam* has a boiling point of ~33 ^{o}C.[22] Another metric in which this trend can also be observed is the volume

occupied per molecule. As pure substances, *ipal* molecule takes up ~7% less volume than *ipam* and similar trend is observed also for other alcohols/amines. [22]

Conclusions

First-order NDIS experiments with H/D substitution on the methyl groups were conducted on 3m aqueous solutions of isopropanol and isopropylamine. The internal coordination number concentration invariance function was calculated to reveal the differences in the hydration of the alcohol and amino groups. Molecular dynamics simulations were then conducted on identical systems to interpret the experimental measurements. The agreement between the simulations and the structural experimental measurements of *ipal* and *ipam* is satisfactory. More detailed analysis of this comparison is complicated by the topology of the investigated molecules. Intrinsically, if H/D substitution experiments are performed on the isopropyl methyl group, there are three H/D substitution locations, that while readily conformationally exchangeable do nonetheless produce different correlations for many of the features of interest in this study. The hydroxy and amino groups are in principal isomorphic in the total number of hydrogen bonds they can form - amine can be the donor of two hydrogen bonds and the acceptor of one, while alcohol can be the donor of one hydrogen bond and the acceptor of two. Using MD simulations we find that the amino group is a better hydrogen bond acceptor than the alcohol is a hydrogen bond donor. This is, however, more than compensated by the fact that the amine is a weaker hydrogen bond donor than the alcohol is a hydrogen bond acceptor. When these two factors are summed up, it is found that the alcohol forms slightly more hydrogen bonds than the amine group. Namely, from the MD simulations, which were consistent with the experimental data, it was found that the amine

group forms about 7 percent less hydrogen bonds than an alcohol on an equivalent isopropyl group.

Acknowledgment

We thank the D4C staff of the Institute Laue Langevin for their help with the neutron scattering experiments. Support from the Czech Science Foundation (grant number P208/12/G016) is gratefully acknowledged. P.J. thanks the Academy of Sciences for the Praemium Academie award. J. H. acknowledges support from the International Max Planck Research School on Dynamical Processes in Atoms, Molecules, and Solids.

References

1. Mason, P. E.; Brady, J. W., "Tetrahedrality" And the Relationship between Collective Structure and Radial Distribution Functions in Liquid Water. *Journal of Physical Chemistry B* **2007,** *111* (20), 5669-5679.
2. Mason, P. E.; Neilson, G. W.; Saboungi, M.-L.; Brady, J. W., The Conformation of a Ribose Derivative in Aqueous Solution: A Neutron-Scattering and Molecular Dynamics Study. *Biopolymers* **2013,** *99* (10), 739-745; Mason, P. E.; Neilson, G. W.; Enderby, J. E.; Saboungi, M. L.; Brady, J. W., Structure of Aqueous Glucose Solutions as Determined by Neutron Diffraction with Isotopic Substitution Experiments and Molecular Dynamics Calculations. *Journal of Physical Chemistry B* **2005,** *109* (27), 13104-13111.
3. Chang, J.; Lenhoff, A. M.; Sandler, S. I., Solvation Free Energy of Amino Acids and Side-Chain Analogues. *Journal of Physical Chemistry B* **2007,** *111* (8), 2098-2106.
4. Klauda, J. B.; Venable, R. M.; Freites, J. A.; O'Connor, J. W.; Tobias, D. J.; Mondragon-Ramirez, C.; Vorobyov, I.; MacKerell, A. D., Jr.; Pastor, R. W., Update of the Charmm All-Atom Additive Force Field for Lipids: Validation on Six Lipid Types. *Journal of Physical Chemistry B* **2010,** *114* (23), 7830-7843.
5. Bryantsev, V. S.; Diallo, M. S.; Goddard, W. A., III, Pk(a) Calculations of Aliphatic Amines, Diamines, and Aminoamides Via Density Functional Theory with a Poisson-Boltzmann Continuum Solvent Model. *Journal of Physical Chemistry A* **2007,** *111* (20), 4422-4430.
6. Nagy, P. I.; Erhardt, P. W., On the Interaction of Aliphatic Amines and Ammonium Ions with Carboxylic Acids in Solution and in Receptor Pockets. *Journal of Physical Chemistry B* **2012,** *116* (18), 5425-5436.
7. Fedotova, M. V.; Kruchinin, S. E., Hydration of Methylamine and Methylammonium Ion: Structural and Thermodynamic Properties from the Data of the Integral Equation Method in the Rism Approximation. *Russian Chemical Bulletin* **2012,** *61* (2), 240-247; Rizzo, R. C.; Jorgensen, W. L., Opls All-Atom Model for Amines: Resolution of the Amine Hydration Problem. *Journal of the American Chemical Society* **1999,** *121* (20), 4827-4836; Wan, S. Z.; Stote, R. H.; Karplus, M., Calculation of the Aqueous Solvation Energy and Entropy, as Well as Free Energy, of Simple Polar Solutes. *Journal of Chemical Physics* **2004,** *121* (19), 9539-9548.

8. Hesske, H.; Gloe, K., Hydration Behavior of Alkyl Amines and Their Corresponding Protonated Forms. 1. Ammonia and Methylamine. *Journal of Physical Chemistry A* **2007,** *111* (39), 9848-9853.
9. Foglia, F.; Lawrence, M. J.; Lorenz, C. D.; McLain, S. E., On the Hydration of the Phosphocholine Headgroup in Aqueous Solution. *Journal of Chemical Physics* **2010,** *133* (14), 10.
10. Neilson, G. W.; Enderby, J. E., The Structure of an Aqueous-Solution of Nickel Chloride. *Proceedings of the Royal Society of London Series a-Mathematical Physical and Engineering Sciences* **1983,** *390* (1799), 353-371.
11. Mason, P. E.; Neilson, G. W.; Dempsey, C. E.; Price, D. L.; Saboungi, M. L.; Brady, J. W., Observation of Pyridine Aggregation in Aqueous Solution Using Neutron Scattering Experiments and Md Simulations. *Journal of Physical Chemistry B* **2010,** *114* (16), 5412-5419.
12. Fischer, H. E.; Cuello, G. J.; Palleau, P.; Feltin, D.; Barnes, A. C.; Badyal, Y. S.; Simonson, J. M., D4c: A Very High Precision Diffractometer for Disordered Materials. *Appl. Phys. A-Mater. Sci. Process.* **2002,** *74*, S160-S162.
13. Soper, A. K.; Neilson, G. W.; Enderby, J. E.; Howe, R. A., Neutron-Diffraction Study of Hydration Effects in Aqueous-Solutions. *Journal of Physics C-Solid State Physics* **1977,** *10* (11), 1793-1801.
14. Enderby, J. E.; Cummings, S.; Herdman, G. J.; Neilson, G. W.; Salmon, P. S.; Skipper, N., Diffraction and the Study of Aqua Ions. *Journal of Physical Chemistry* **1987,** *91* (23), 5851-5858.
15. Case, D. A.; Darden, T. A.; Cheatham, T. E.; Simmerling, C. L.; Wang, J.; Duke, R. E.; Luo, R.; Walker, R. C.; Zhang, W.; Merz, K. M.; Roberts, B.; Wang, B.; Hayik, S.; Roitberg, A.; Seabra, G.; Kolossvary, I.; Wong, K. F.; Paesani, F.; Vanicek, J.; Liu, J.; Wu, X.; Brozell, S. R.; Steinbrecher, T.; Gohlke, H.; Cai, Q.; Ye, X.; Hsieh, M. J.; Cui, G.; Roe, D. R.; Mathews, D. H.; Seetin, M. G.; Sagui, C.; Babin, V.; Luchko, T.; Gusarov, S.; Kovalenko, A.; Kollman, P. A., In Amber 11.
16. Jorgensen, W. L.; Tirado-Rives, J., Potential Energy Functions for Atomic-Level Simulations of Water and Organic and Biomolecular Systems. *Proceedings of the National Academy of Sciences of the United States of America* **2005,** *102* (19), 6665-6670.
17. Berendsen, H. J. C.; Grigera, J. R.; Straatsma, T. P., The Missing Term in Effective Pair Potentials. *Journal of Physical Chemistry* **1987,** *91* (24), 6269-6271.
18. Berendsen, H. J. C.; Postma, J. P. M.; Vangunsteren, W. F.; Dinola, A.; Haak, J. R., Molecular-Dynamics with Coupling to an External Bath. *Journal of Chemical Physics* **1984,** *81* (8), 3684-3690.
19. Essmann, U.; Perera, L.; Berkowitz, M. L.; Darden, T.; Lee, H.; Pedersen, L. G., A Smooth Particle Mesh Ewald Method. *Journal of Chemical Physics* **1995,** *103* (19), 8577-8593.
20. Mason, P. E.; Neilson, G. W.; Dempsey, C. E.; Brady, J. W., Neutron Diffraction and Simulation Studies of Csno3 and Cs2co3 Solutions. *Journal of the American Chemical Society* **2006,** *128* (47), 15136-15144.
21. Mason, P. E.; Neilson, G. W.; Price, D. L.; Saboungi, M.-L.; Brady, J. W., A New Structural Technique for Examining Ion-Neutral Association in Aqueous Solution. *Faraday Discussions* **2013,** *160*, 161-170.
22. Lide, E. D. R., Handbook of Chemistry and Physics. 86th ed.; 2005-2006; pp 3-314, 3-442.